Following the Density evolution using Real Time Density Functional Theory and Density Based indexes: application to model push-pull molecules

Feven Alemu Korsaye, Aurélien de la Lande, Ilaria Ciofini

Following the Density evolution using Real Time Density Functional Theory and Density Based indexes: application to model push-pull molecules

F. A. Korsaye[1,2], A. de la Lande[2,*], I. Ciofini[1,*]

[1] *PSL University, CNRS, Chimie ParisTech-PSL, Institute of Chemistry for Life and Health Sciences (i-CLeHS), Theoretical Chemistry and Modelling Group (CTM), 75005 Paris, France*
[2] *Institut de Chimie Physique, Université Paris Saclay, CNRS, UMR 8000. 15 avenue Jean Perrin, 91405, Orsay France*

Abstract

Considering as test case a family of organic rod like push-pull molecules, we derived and applied density based index enabling the description and diagnostic of the electronic density evolution in Real Time Time Dependent Density Functional Theory (RT-TDDFT) simulations.
In particular, both the Charge Transfer (CT) distance and a diagnostic index, the D_{CT} and M_{AC}^{RT} respectively, were computed on the fly from the density distribution obtained at a given time and the reference ground state density and their mean values were compared to what obtained at Linear Response-TDDFT level.
Besides giving a way of analyzing the density redistribution occurring in time, these tools allowed to show how RT-TDDFT, which is definitely a powerful method to model the evolution of the density in charge transfer or charge separation processes, can be affected by the same artifacts known for LR-TDDFT approaches and, particularly, to those related to the use of approximate exchange correlation functionals. The analysis here performed allowed to identify and discard on fly the electronic configurations corresponding to spurious situations.

Keywords: DFT and TDDFT; RT-TDDFT; density based descriptors; Charge Transfer excited states

1. Introduction

Density Functional Theory (DFT)[1] and Time-dependent DFT (TDDFT)[2] are amongst the most widespread quantum chemical methods currently available allowing the description of ground and excited states properties of molecules. This wide application derives mainly from their simple formalism and their very good accuracy to computational cost ratio, that make these methods reliable also for the description of the properties of medium to large size molecular systems[3].

Linear response TDDFT within the Casida's formalism (LR-TDDFT)[4] is probably the most employed formulation of TDDFT and, as the acronym suggests, it consists in retaining only the linear response of the electron density to the applied perturbation, enabling in such a way the computation of properties directly related to the optical spectra of molecules.[5] Real-time TDDFT (RT-TDDFT)[6,7] denotes another methodology where the application of the perturbation is followed by the propagation of the electron density via numerical integration. The perturbation may fall in the linear response regime but is in principle not restricted to it.

RT-TDDFT has been largely used to model electron dynamics in molecular systems, to simulate the electron density reorganization or to analyze excited states evolution in time[8,9]. Furthermore, by applying a strong electric field, it also possible to simulate non-linear optical phenomena such as ionization of molecules[10]. Simulations may be carried out for molecules in the gas phase, but it is eventually possible to simulate the environment explicitly for example by means of the coupling between RT-TDDFT and polarizable force fields[11].

Nonetheless, whatever of these two formalisms is chosen, the drawbacks related to the underlying DFT approach impact the reliability of the results. In particular, it is now well documented that TDDFT methods suffer from an intrinsic drawback related to the description of excited state with long-range Charge Transfer (CT) character or, more generally, of localized charge separated states[12,13,14,15]. Many studies have demonstrated that DFT based approaches fail to reproduce the correct 1/R asymptotic behavior (with R the distance between the transferred electron and the generated hole) due to the approximated nature of the exchange and correlation functional (XC) used to express the total energy of the system[16,17,18,19,20,21,22,23]. As a consequence, CT excited states energies are to some extent underestimated, depending on the level of approximation used for the XC functional. In particular, previous LR-TDDFT studies have shown how, using Local-Density Approximation (LDA)[24,25] or Generalized Gradient Approximation (GGA)[26,27,28] functionals, the

energies of CT excited states are usually underestimated, while the functionals that incorporate a fraction of exact exchange, such as Global Hybrids (GH)[29,30] or, Range Separated Hybrids (RSH)[31,32] functionals, mitigate this error. Even more severely, some of these functionals may predict the presence of unphysical dark states, known as ghost states, that lye at very low energies and thus providing a misleading picture of the photophysics of the molecules considered[17].

Various tools and indexes allowing to estimate the reliability of TDDFT in addressing CT processes have been developed over the last decades[33,34,35]. Furthermore, several methods have been developed to analyze the nature of excited states in terms of their charge transfer character[36,37,38,39, 40,41,42,43,44].

In this context, some of us were involved in the development of density-based indexes to quantify charge transfer distance, leading to the so-called D_{CT} family of index[36,37,38]. The index in its original and simplest formulation[36] quantifies, in a simple and intuitive way, the degree of locality of an excitation by computing the distance between the barycenter of the hole and electron charge distribution after excitation. Once this distance, indicated as D_{CT}, is defined, beside having a quantitative measure of the local character of the transitions, it is also possible to define an estimate of the lower bound of the associated transition energy using the so-called M_{AC} index[34,35]. In this way is possible to spot both spurious and ghost CT excited states.

The purpose of this work is to show how these two indexes can be generalized and computed in the context of RT-TDDFT in order to describe and diagnostic electronic density evolution upon real time propagation. In addition, the results collected from RT simulations and LR calculations can also be compared using the same descriptors.

More generally, the present work aims to proof and validate the use of the density-based descriptors into the RT-TDDFT formulation and to test their applicability as diagnostic tools in the electron dynamics domain.

As a test case, we consider a family of simple rod-like push-pull compounds, depicted in Scheme 1, which have been already largely studied by LR-TDDFT[34,36].

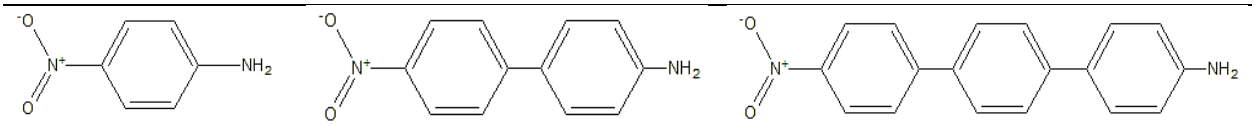

Scheme 1. The family of molecule considered as test case in the present work.

Indeed, these molecules are typical push-pull systems containing two groups, one acting as electron donor ($-NH_2$) and another playing the role of electron acceptor ($-NO_2$), connected via a spacer of different length. All these molecules are expected to show an excited state with a significant CT character as a result of a one electron excitation from the donor ($-NH_2$) to the acceptor ($-NO_2$). Nonetheless, possible delocalization over the bridge will modulate this ideal CT phenomenon and eventually reduce the spatial extent of the CT.

In order to magnify the presence of ghost states, we consider in the present case, only an LDA exchange correlation functional for which we expect, in analogy with LR-TDDFT calculations, the highest occurrence of ghost states during the RT simulation.

The paper is structured as it follows: in the "Computational methods and details" are reported the theoretical background of the RT-TDDFT formalism and in the "Density based index for the description of RT-DFT densities" the definition of the D_{CT} and M_{AC} indexes together with the formulation of this latter allowing its evaluation in the RT formalism ($M_{AC}(t)^{RT}$). The results obtained from the electron dynamic simulations are collected and commented in the section "Results and Discussion", while in the last section some future perspectives concerning the possible use of these two descriptors in the RT domain are discussed.

2. Computational methods and details

We carried out all RT and LR TD-DFT calculations using developer versions of the deMon2k software[45,46] (versions 4.4.5 and 6.0.8 respectively for RT-TDDFT[11] and LR-TDDFT[47] simulations) using the local SVWN[24,25] exchange and correlation functional. deMon2k implements Kohn-Sham DFT in the context of Auxiliary Density Functional Theory (ADFT) approach[47,48]. The ADFT approach relies on variational density-fitting (DF)[49] to avoid the calculation of four center electron repulsion integrals (ERIs) appearing in the electronic energy expression. This is made possible defining beside the Kohn-Sham (KS) density, built on the KS molecular orbitals, an auxiliary density, built as a linear combination of auxiliary functions. Using the auxiliary density, it is possible to express the total KS energy and potential only in terms of two or three-centers ERIs. In the ADFT framework, this fitted density is also adopted to compute ad approximate exchange and correlation potential energy. This approximation becomes particularly beneficial in the case of RT simulations where a different KS density is formed at every propagation step, thus allowing to reduce the computational cost of the simulations without altering the stability and accuracy of the propagation[11,50]. In the present work the automatically

generated auxiliary basis set GEN-A2*[51] was adopted for both LR calculations and RT simulations, together with the basis set 6-31+G(d).

It should be noted that, although the auxiliary fitted density could in some cases provide for a reliable accuracy[52], in this work this latter was used only to calculate an approximate electronic repulsion interaction and an exchange and correlation energy, while the DCT analysis has been carried out using the KS density computed on-the-fly during the simulations. .

Two distinct approaches can be considered to trigger electron dynamics in the system from a ground state density. One may apply an appropriate electric field pulse to excite the ground state electron density so as to ensure a full inversion of population to the desired excited state. Alternatively, one can prepare the electronic system to a desired excited state by depopulating occupied Kohn-Sham orbitals and populating vacant ones. Each approach has its pro and cons. In particular, the former would in principle require non-adiabatic XC functionals that incorporate memory effects to properly describe state-to-state transitions.[53,54,55,56]. In any case non-adiabaticity plays a minor role with respect to the nature of the exchange correlation functional used. In this work, all the simulations reported have been conducted following the approach involving the application of an appropriate perturbation that brings the system at the desired excite state energy. This rational pulse design can be obtained operating on the applied electric field intensity and envelop accordingly to the so-called *π-pulse* condition[57]:

$$\overrightarrow{\mu_{0n}}\overrightarrow{F_0}\int_{-\infty}^{+\infty} s(t)\,dt = \hbar\pi \qquad (1)$$

Where $\overrightarrow{F_0}$, s and $\overrightarrow{\mu_{0n}}$ are respectively the vector containing the maximal amplitude of the electric field, the envelop of the pulse and the transition dipole moment connecting the ground state (S_0) to the targeted excites state n (S_n). For the envelop s, we chose a cos^2-shaped function, that, compared to the gaussian-shaped pulse, ensures more easily to fulfill the zero-pulse-area-condition (ZPAC, $\int_{t=0}^{t_{max}} \vec{F}(t) = 0$[58]). Finally, the frequency of the electric field, which coincides with the targeted transition energy $S_0 \rightarrow S_n$, can be obtained from the absorption spectrum computed for the molecule. This spectrum is obtained from RT simulations in which an ultrafast electric field (a "*kick"*) is applied in each of the three x, y and z directions. Such kicks excite the electronic cloud in all the accessible excited states. The polarizability tensor is then obtained by Fourier transformation of the resulting molecular dipole moment[9,59].

After setting the electric field pulse, the electron density is propagated in time-domain via numerical integration on attosecond timescale. To this end, a propagator should be selected on the basis of its stability and performance criteria. We adopted for our simulations the second-order Magnus propagator (SOMP)[60,61]. Conceptually, the time dependent electron density matrix $\boldsymbol{P}$, at time $t+\Delta t$ is expressed from its value at time t:

$$\boldsymbol{P}(t+\Delta t) = \boldsymbol{U}(t+\Delta t, t)\, \boldsymbol{P}(t)\, \boldsymbol{U}^{+}(t+\Delta t, t) \qquad (2)$$

where $\boldsymbol{U}$ is the evolution operator and $\boldsymbol{U}^{+}$ its complex conjugate. Its form in the SOMP algorithm is defined as follow:

$$\boldsymbol{U}(t+\Delta t, t) = e^{-i\boldsymbol{H}(t+\frac{\Delta t}{2})\Delta t} \qquad (3)$$

As shown, the propagation of the electron density at time t requires the knowledge of the KS operator value at time $\boldsymbol{H}(t+\Delta t/2)$. The method here adopted for its evaluation is known as predictor-corrector (PC) method[62]. Note that in eqn 2 and 3, both $\boldsymbol{P}$ and $\boldsymbol{H}$ are expressed in an orthonormal MO basis. The working principle of the algorithm can be briefly showed in 5 steps:

1. Initial guess of $\boldsymbol{H}(t_n + \frac{\Delta t}{4})$ by extrapolation from $\boldsymbol{H}(t_{n-1} + \frac{\Delta t}{2})$ and $\boldsymbol{H}(t_{n-2} + \frac{\Delta t}{2})$.
2. Propagation of $\boldsymbol{P}(t_n)$ to $\boldsymbol{P}(t_n + \frac{\Delta t}{2})$ using $\boldsymbol{H}\left(t_n + \frac{\Delta t}{4}\right)$.
3. Construction of KS potential $\boldsymbol{H}(t_n + \frac{\Delta t}{2})$ from $\boldsymbol{P}(t_n + \frac{\Delta t}{2})$.
4. Propagation of $\boldsymbol{P}(t_n)$ to $\boldsymbol{P}(t_n + \Delta t)$ using $\boldsymbol{H}(t_n + \frac{\Delta t}{2})$.
5. Subsequent propagation using the KS potentials at time $(t_n + \frac{\Delta t}{2})$ and $(t_{n-1} + \frac{\Delta t}{2})$.

A non-trivial and time-consuming point during the density propagation is the evaluation of the exponential of the Hamiltonian matrix involved in the Magnus propagator. Matrix exponentiation has been calculated by diagonalization of the Hamiltonian matrix. The timestep was set to 1.0 attosecond and the simulations were pursued for 10 femtoseconds after the end of the pulse.

3. Density based index for the description of RT-DFT densities

With the aim of analyzing the electron density evolution, a new density-based descriptor has been developed here and applied to characterize excited states. This latter is derived from the original M_{AC} index which was adapted to be computed on top of RT simulations. As already mentioned, the D_{CT} index[36] is able to quantify the degree of locality of a CT process, by giving an estimate of the hole-electron separation at the excited state. Its development was originally motivated by the need of providing a condensed and quantitative measure of a CT phenomenon, beside an orbital

based description. To this end, the index quantifies the hole-electron distance on the basis of the difference in density distributions between the ground and excited state of interest. This procedure, as reported in ref 36 consists of 4 steps:

1. Computation of electron density variation as difference between ground and excited state density: $\Delta\rho(\boldsymbol{r}) = \rho_{ES}(\boldsymbol{r}) - \rho_{GS}(\boldsymbol{r})$.
2. Definition of two charge distributions corresponding to the region in space associated, respectively, to an electron density increment ($\rho_+(\boldsymbol{r})$) and depletion ($\rho_-(\boldsymbol{r})$).
3. Computation of the barycenters of these two charge density distributions ($\boldsymbol{R}_+$and $\boldsymbol{R}_-$).
4. Evaluation of the charge transfer distance as distance between these barycenters: $D_{CT} = |\boldsymbol{R}_+ - \boldsymbol{R}_-|$.

As the D_{CT} value can be estimated directly from difference in density between ground and excited state, this index can be directly computed on selected snapshots along a RT simulation trajectory as the difference in density between the actual propagated density and the ground state initial density. In this case, the computed D_{CT} values along the RT trajectory reflect the evolution of the electron density reorganization.

As mentioned in Introduction, the D_{CT} index has been used to give an estimate of a lower bound for the energy of the CT transition using another index, the MAC (*Mulliken averaged configuration*)[35], derived from the Mulliken formula[63] originally proposed to estimate the energy for intermolecular CT excitations. This index has been used to diagnostic ghost and spurious states arising in TDDFT calculations both in the case of model push-pull systems[34] and organometallic complexes[35].

The starting point for the derivation of the MAC index is the Mulliken formula allowing to evaluate the lower bound for the excitation energy (ω_{CT}) in the case of a net one electron intermolecular CT between a donor (D) and acceptor (A) placed at distance R:

$$\omega_{CT} = IP_D - EA_A - \frac{1}{R} \qquad (4)$$

Here $\mathrm{IP_D}$ is the ionization potential of the donor, $\mathrm{EA_A}$ the electron affinity of the acceptor while 1/R represent the hole-electron coulombic interaction after CT.

Relying on this equation, some of us have recently proposed a way to estimate the ω_{CT} directly for any TDDFT calculations, using a Koopman type approach: IP_D and EA_A are replaced by the weighted averaged of the starting (ϵ_{i}) and final (ϵ_{a}) HF orbital energies computed using the converged SCF KS orbitals ($\epsilon_{\mathrm{a}}^{\mathrm{DFT-HF}}$) and ($\epsilon_{\mathrm{i}}^{\mathrm{DFT-HF}}$), respectively. The geometrical distance

between the D and the A groups (R) is estimated from the D_{CT} value. The resulting M_{AC} expression for a LR-TDDFT calculation thus reads:

$$M_{AC} = \frac{\sum_{ia}[C_{ia}{}^2(\epsilon_a{}^{DFT-HF} - \epsilon_i{}^{DFT-HF})]}{\sum_{ia} C_{ia}{}^2} - \frac{1}{D_{CT}} \quad (5)$$

where the weights c_{ia} are the CI coefficients obtained as solutions of TDDFT equations[4].

Here, the use of single-cycle HF orbital energies ($\epsilon_a{}^{\text{DFT-HF}}$ and $\epsilon_i{}^{\text{DFT-HF}}$) on the converged DFT orbitals allows to correct their possible underestimation due to Self-Interaction-Error.

The M_{AC} can be thus used to identify unphysical states in TDDFT: if a given TDDFT transition has an energy greater than the related M_{AC} energy, it is associated to a real state, while a TDDFT energy lower than the M_{AC} index will identify a ghost or a spurious state.

$$E^{TD-DFT} > M_{AC} \rightarrow Real\ State; \quad E^{TD-DFT} < M_{AC} \rightarrow Ghost\ State. \quad (6)$$

In order to compute the M_{AC} index in the case of RT-TDDFT simulations, some modifications are needed in eqn. 5. In particular, the density reorganization during the simulation, will now be expressed as a function of the occupation number of the occupied and virtual orbitals along the dynamic, preserving a fixed total number of electrons. This formulation leads to the following expression for the index adapted for electron dynamic simulations at time t_j:

$$M_{AC}^{RT}(t_j) = \frac{\sum_{virt}[n_{virt}(t_j)\epsilon_{virt}{}^{DFT-HF}] - \sum_{occu}[n_{occu}(t_j)\epsilon_{occ}{}^{DFT-HF}]}{\sum_{virt} n_{virt}(t_j) + \sum_{occu} n_{occu}(t_j)} - \frac{1}{D_{CT}(t_j)} \quad (7)$$

where ϵ_{virt}^{DFT-HF} and ϵ_{occu}^{DFT-HF} are respectively the eigenvalues of the contributing virtual and occupied molecular orbitals with single-cycle HF correction, while $n_{virt}(t_j)$ and $n_{occu}(t_j)$ are the related occupation number at time t_j. The energies of the molecular orbitals at HF level of theory are obtained using Gaussian 16 software, while the time step considered to extract on-the-fly the occupation numbers is 20 attoseconds, the same used to evaluate the density and compute the D_{CT} index. Finally, comparing the set of energy values from $t_{initial}$ to t_{final} with the CT state energy, it is possible to assess which regions of the electron dynamic simulation derives from a correct or erroneous description of the process.

Results and Discussion

The RT and LR results obtained for the three model systems reported in Scheme 1 will be discussed in the following. First an analysis of the full absorption spectra of these molecules has been

performed via a RT-TDDFT simulation, that involves the application of a sudden electric filed in the very first propagation steps (*kick*) allowing to excite all the electronic frequencies simultaneously. The simulations are carried out for the three directions of polarization and the resulting densities are propagated in time. The Fourier transformation of the field-free time dependent dipole moment gives the polarizability tensor in the frequency domain and allows to construct the desired spectrum. These spectra for the three molecules are reported in Figure 1 and they are compared with those obtained with the LR approach. Remember we work in both case under a linear response regime so that both approaches should give similar results. The acronym LR is actually used here to refer to Casida's formulation of TDDFT, not to emphasize any non-linear behavior in our RT-TDDFT propagations.

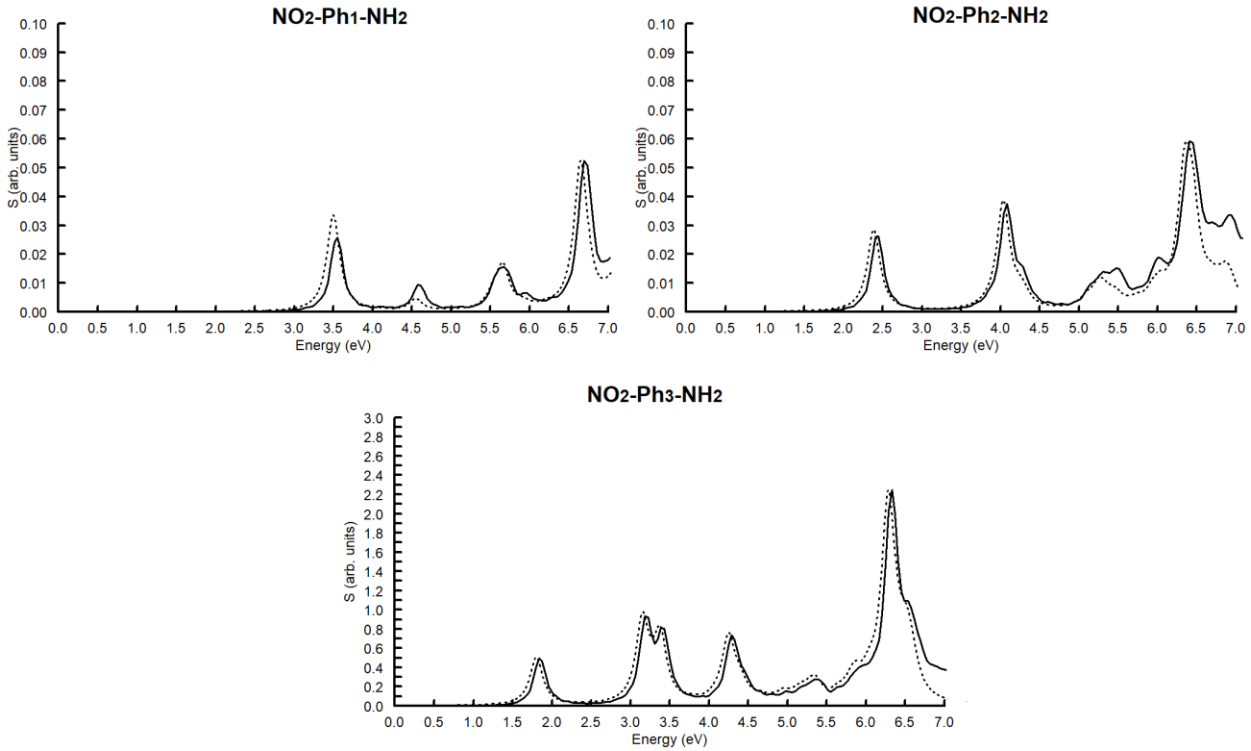

Figure 1 Spectra obtained RT (full-line) and LR (dashed-line) simulations RT simulations were performed applying a kick with 0.005au= 2.5 x 10^3 mV/nm intensity while the density has been propagated every Δt=1as for a total simulation time of 25fs. Before the Fourier transformation the peaks have been broadened by damping the time signal by $e^{-(t/\tau)}$ with τ=300au=7.26fs. LR-TDDFT spectra were obtained broadening the computed excitations with Gaussians of width 0. 2eV. The LR spectra have been normalized with respect to the most intense peaks of the corresponding RT spectrum

s	λ_{max} (eV)		D_{CT} (Å)				d(N-N) (Å)
	RT	LR	LR	RT^{MAX}	RT^{MEAN}	$RT^{MEAN-corr}$	
NO_2-(Ph)$_1$-NH_2	3.56	3.50	1.99	2.75	1.54	1.10	5.57
NO_2-(Ph)$_2$-NH_2	2.45	2.39	3.72	3.59	1.96	1.11	9.89
NO_2-(Ph)$_3$-NH_2	1.85	1.80	5.67	5.34	2.74	1.21	14.19

Table 1. Computed λ_{max} associated to the lowest energy band derived from LR and RT spectra and associated charge transfer distance D_{CT} RT^{MAX}, RT^{MEAN} and $RT^{MEAN\text{-}corr}$ are the maximum, mean and corrected mean values of charge transfer distance computed from the RT simulation (see text for explanation). d(N-N) is the geometrical distances between the donor and acceptor units (distance between the two N atoms at the optimized ground state geometry).

The comparison between the absorption energies in the UV-Vis region computed at RT-TDFFT (full-line) and LR-TDDFT (dashed-line) level allows to show that these methods provide an analogous spectral prediction, with a mean difference of λ_{max} around 0.05 eV for the three molecules (the comparison of all the LR and RT transitions energies in the UV-Vis region is reported in the Supporting Information). In particular, the lowest energy peaks of the three spectra arise from a single excited state corresponding to the CT excitations, as it can be easily estimated from the analysis of the associated D_{CT} values reported in Table 1.

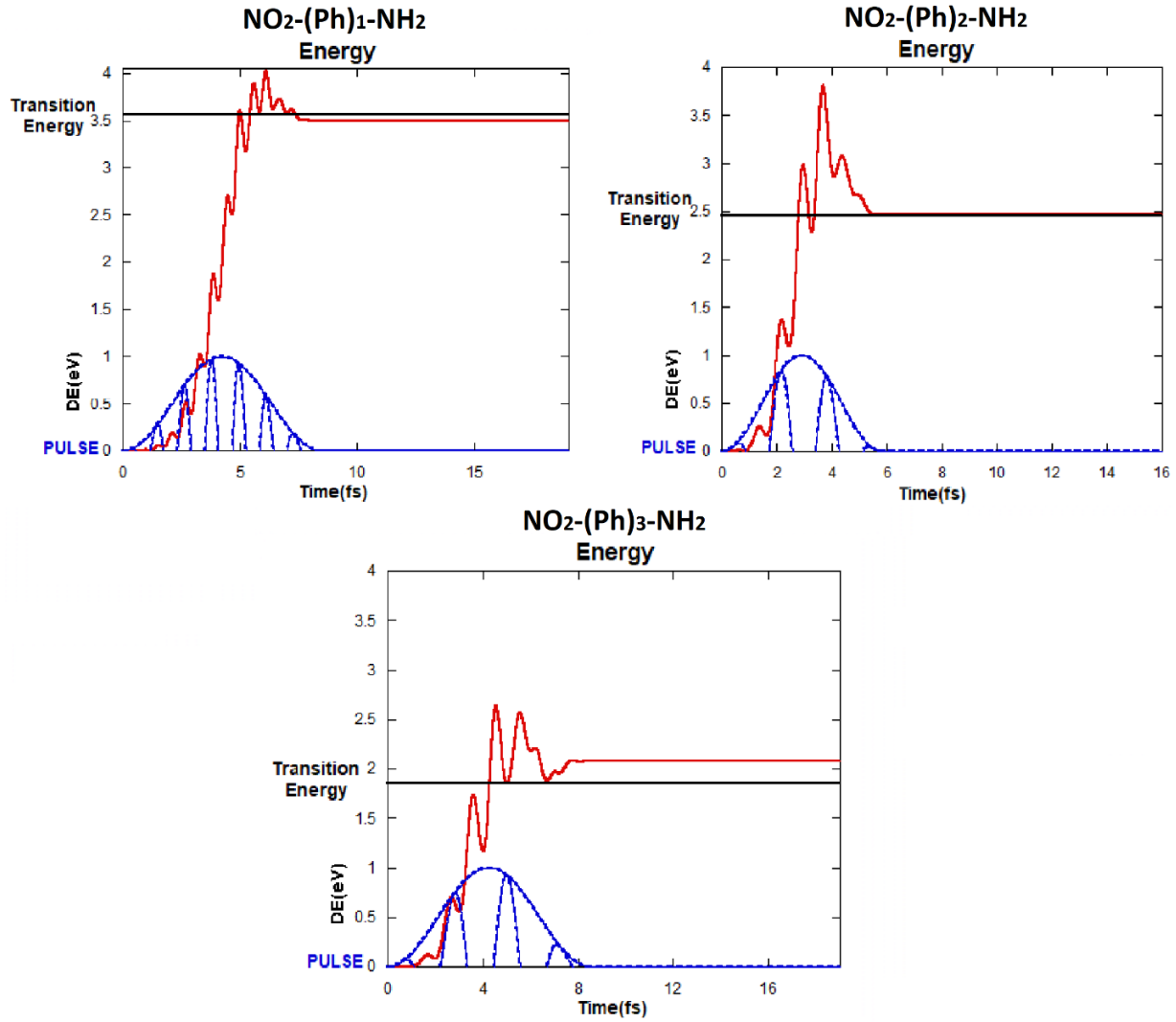

Figure 2 Energy differences (E (simulation) – E (ground state)) during the RT simulations (red) and vertical transition energies obtained from the LR spectra (black). In blue, the applied $\cos^2$-shaped pulse.

Next, these RT energies associated to the CT states have been used to set up a pulse enabling an inversion of population from the ground to the targeted excited state. The energy evolution computed for the three molecules during the simulations (red) together with the applied pulse evolution (blue) are reported in Figure 2. As expected, a stabilization of the energy is achieved right after the end of the pulse and the comparison of these values with the corresponding excited state energies obtained from the RT spectra show that we were able to effectively reach a reasonable population of the targeted charge transfer state.

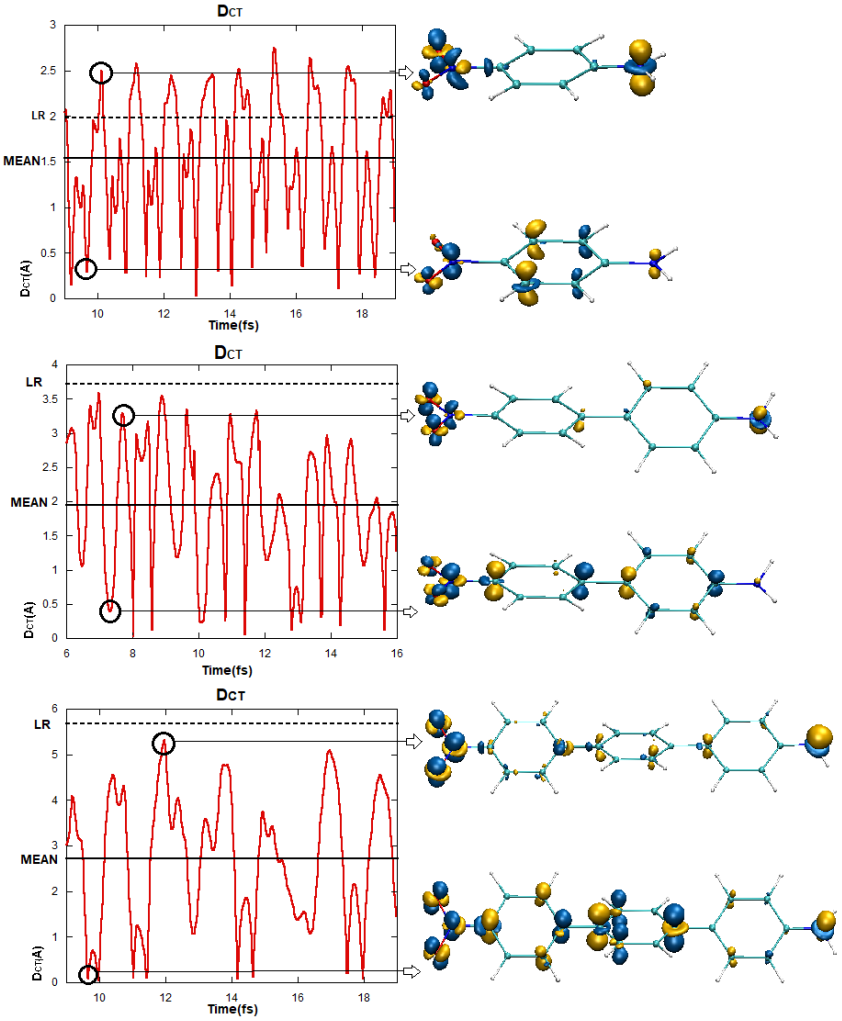

Figure 3. On the left panels, computed Charge transfer distance fluctuation computed after the end of the perturbation for the three molecules. In black line the D_{CT} mean value obtained from the RT simulation and in dashed line the D_{CT} value computed via the LR approach. On the right panel the ground to excited state electron density difference corresponding to the maximum and minimal values computed during the RT simulations. The regions corresponding to an electron density increment are showed in blue, while those with a density depletion are depicted in yellow (isosurface value ±0.007 au).

An analysis of the evolution of the hole-electron distance during the dynamics has been performed considering the difference between the density at a given time and the reference ground state

density to compute the D_{CT}. In Figure 3 are reported the D_{CT} values computed for the three molecules together with the density difference computed on selected snapshots. Since the applied perturbations determine a redistribution of the electron densities, the resulting D_{CT} values fluctuate between values close to zero, characteristic of a locally excited state, and values close to the donor (-NH_2) to acceptor (-NO_2) geometrical distance corresponding to a situation of net Charge Transfer. Therefore, not surprisingly, the highest D_{CT} values are computed in the case of the molecule possessing the longest spacer.

The presence of the phenyl groups plays a key role on the periodicity of the charge redistribution: comparing the result obtained for the three molecules, one may notice how the frequency of the D_{CT} oscillation depends on the size of the molecule. Increasing the number of the phenyl groups in the bridge between the donor and the acceptor units, this frequency decreases. In particular, the active role of the phenyl groups as well as the possible delocalization process can be inferred analyzing the charge transfer distance computed using the LR and RT approach as well as the geometrical distance between the donor and the acceptor units (see Table 1). In the case of the RT approach both the maximal and the mean values of D_{CT} computed along the trajectory can be considered. Comparing the geometrical donor to acceptor group distances to both LR and mean RT D_{CT} values, it is easy to realize that the electron density is largely delocalized on the phenyl spacers, thus determining a significant reduction of the estimated hole-electron distance with respect to an ideal one electron transfer. These results are consistent with previous studies reported in the literature[37,64] also considering the behavior of different functionals or analyzing the effect of the nature of the bridge[65] in the delocalization process. Finally, the mean values of the CT lengths during the RT simulations result to be different compared to the LR ones, since the last derive from a vertical excitation that does not take into account the dynamical nature of the process. Indeed, as a consequence of this, a greater length of the delocalization bridge results in an increase of the deviation between the LR and RT data (see Table 1).

As latest analysis, the computed D_{CT} values were used to evaluate the $M_{AC}(t)^{RT}$ diagnostic index on-the-fly as detailed in the previous section using eqn. 7. The comparison of the computed M_{AC} index to the energy obtained during the RT simulation allowed to spot potential spurious states appearing during the dynamics. In Figure 4, the red points correspond to RT energies that are

expected to be incorrectly described on the basis of the M_{AC} analysis while the green ones to energies correctly described.

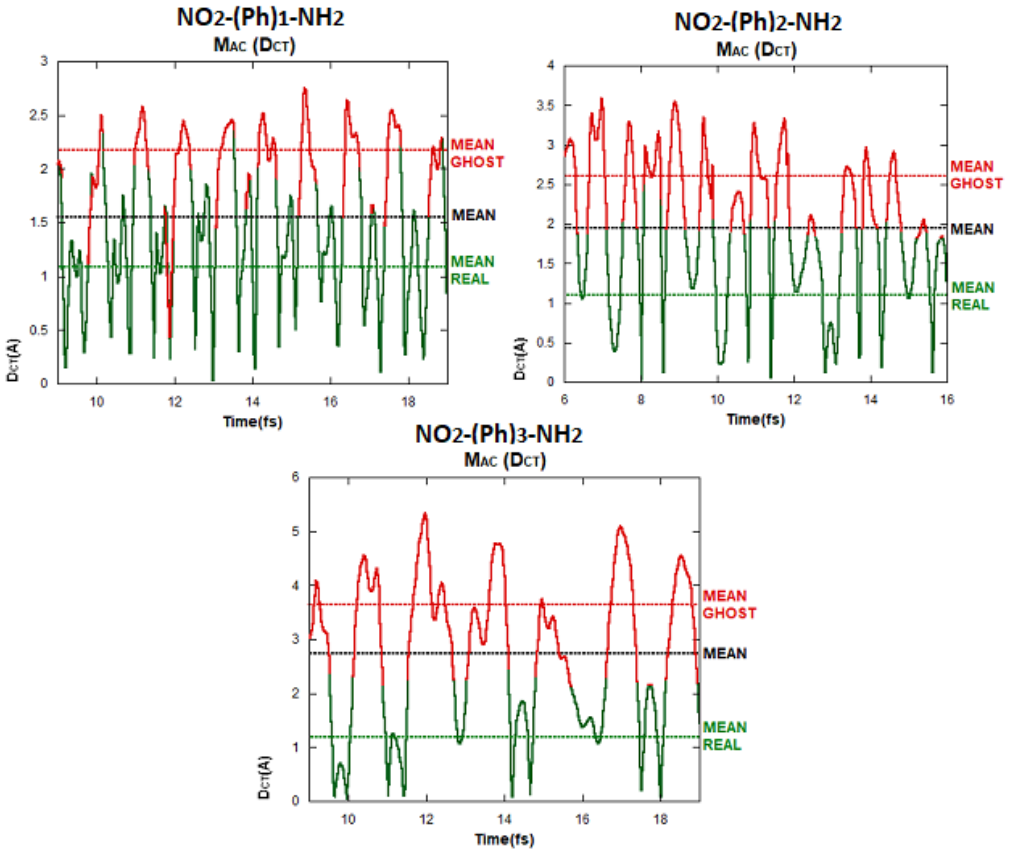

Figure 4. CT distance (Å in the regions of the simulation corresponding to real (green) and ghost states (red). Mean CT distance considering all data points of the simulation (dashed line in black), mean CT length values derived from the ghost (dashed line in red) and real states (dashed line in green) for the three molecules.

*	**LR**	**RT**
NO_2-(Ph)$_1$-NH_2	Real	58.6 % Real
NO_2-(Ph)$_2$-NH_2	Ghost	56.2 % Ghost
NO_2-(Ph)$_3$-NH_2	Ghost	61.9 % Ghost

Table 2. Nature of the excited states considered during LR and RT approach.

Overall, one can remark that the percentage of densities during the simulation corresponding to ghost is higher in the case of the molecules with 2 (56%) and 3 (62%) spacers while in the case of the NO_2-(Ph)$_1$-NH_2 it corresponds roughly to 41%. This agrees with LR calculations showing in the case of NO_2-(Ph)$_2$-NH_2 and NO_2-(Ph)$_3$-NH_2 the presence of a low-lying CT ghost state while this is not the case for NO_2-(Ph)$_1$-NH_2.

Not surprisingly, density distributions corresponding to lower values of the hole-charge distance, describing basically a situation where the LE state is predominant over a CT one and thus characterized by an electron density variation delocalized over the whole molecule, are those related to a correct energy prediction for all the three molecules. On the other, density distribution characterized by a very high D_{CT} distance are those including larger contribution from ghost CT states, thus leading to an overall unphysical description of the density evolution. Comparing the mean D_{CT} values computed on the entire simulation (dashed line in black) with the mean D_{CT} values derived from ghost (dashed line in red) and real (dashed line in green) RT points, it is possible to conclude that most of the electron density configurations of the molecule during the simulation derives from a real states for the first molecule and from ghost states for the second and third molecules. This result can be easily quantified by the percentage of ghost and real states during the simulations reported in Table 2.

Moreover, we can see that if one considers the corrected mean D_{CT} value that is the one obtained from non-ghost states during RT simulation (that is $D_{CT}^{MEAN\text{-}corr}$ in Table 1) very similar values are obtained for independently of the bridge length further confirming a significant delocalization over the phenyl spacers. As expected, the LR and the RT descriptions are indeed similarly affected by the presence of ghost states.

4. Conclusions

In this work we have proposed a new formulation of the D_{CT} and M_{AC} density-based index with the aim of describing and analyzing the reliability of the electronic density evolution computed during RT-TDDFT simulations. We have shown how both these indexes can be computed on the fly from the density distribution obtained at a given time and the reference ground state density and compared their mean values to what computed at LR-TDDFT level.

The analysis of performed shows that a periodic charge redistribution is taking place with periodicity depending on the donor-acceptor distances due to possible charge delocalization over the bridge. This allows the population of states with predominant local excited state character and CT character. The use of the D_{CT} index has allowed to quantify the time evolution of the electronic density while the M_{AC} index has allowed to spot the configurations corresponding to a correct description of the electronic density and those affected by artefacts (ghost states). This analysis thus allows to derived a ‘mean’ CT distance during the simulation that can be corrected after the

elimination of the spurious configurations. Of note for future applications one could use these indexes to filter spurios states in RT-TDDFT simulations.

Of note here model push-pull systems, with increasing donor acceptor distance, and a local exchange and correlation functional (SVWN) were used in order to magnify the presence of ghost states which are known (from LR-TDDFT approaches) to be related to the Self-Interaction-Error and thus cured by the use of functionals with correct asymptotic behavior (GH or RSH). Future work is envisaged to more deeply analyse the effect of the different XC kernels at LR and RT TDDFT level.

More generally, we have shown how the attoseconds electron dynamic simulations which is definitely a powerful method to model the evolution of the density in charge transfer or charge separation processes, can be affected by the same artifacts known for LR-TDDFT approaches and how the two density-based descriptors here proposed may help in the description and diagnostic of the density evolution.

Acknowledgments

We are grateful to Andreas M. Köster and Luis Ignacio Hernandez-Segura for providing us with a developer version implementing their most advanced LR-TDDFT code in the framework of ADFT.

References

1 Parr GR, Yang W (1989) *Density-Functional Theory of Atoms and Molecules Oxford University Press*, USA.
[2] Runge E, Gross E K U (1984) *Phys. Rev. Lett*. 52, 997–1000.
[3] Ulrich CA (2019) *Time-Dependent Density-Functional Theory: Concepts and Applications (Oxford Graduate Texts) Oxford University Press*, USA.
[4] Casida M E. (1995) *Recent Advances in Density Functional Methods*. pp 155–192.
[5] Adamo C, Jacquemin D (2013) *Chem. Soc. Rev*. 42, 845-856.
[6] Calvayrac F, Reinhard P G, Suraud E (1995) Phys. Rev. 15;52(24):17056-17059.
[7] Yabana K, Bertsch GF (1996) *Phys. Rev.* 15;52(24):17056-17059.
[8] Petrone A, Lingerfelt D B, Rega N, X Li (2014) *PCCP* 16, 24457-24465.
[9] Lopata K, Govind N (2011) *J. Chem. Theory Comput*. 7, 5, 1344–1355.
[10] Omar K A, Hasnaoui K, de la Lande A, (2021) *Annu. Rev. Phys*. 72 :445-464.
[11] Wu X, C Teuler J-M, Cailliez F, Clavaguéra C, Salahub D R, de la Lande (2017) *A J. Chem. Theory Comput*. 13, 9, 3985–4002.

[12] Dreuw A, Head-Gordon M (2004) *J. Am. Chem. Soc*. 126, 12, 4007–4016.
[13] Magyar R J, Tretiak S, (2007) *J. Chem. Theory Comput*. 3, 3, 976–987.
[14] Cai Z-L, Sendt K, Reimers J R (2002) *J. Chem. Phys*. *117* 5543–5549
[15] Tozer, D. J. (2003). *J. Chem. Phys*. *119*, 12697–12699.
[16] Grimme S, Parac M, (2003) *ChemPhysChem* 17;4(3):292-5.
[17] Dreuw A, Weisman J L, Head-Gordon M, (2003) *J. Chem. Phys. 119*, 2943.
[18] Casida, M E, Jamorski C, Casida K C, Salahub D R (1998) *J. Chem. Phys*. *108*, 4439–4449.
[19] Ottochian A, Morgillo C, Ciofini I, Frisch M J, Scalmani G, Adamo C, (2020) *J. Comput. Chem. 41*, 1242–1251.
[20] Casanova-Páez M, Goerigk L, (2020) *J. Chem. Phys. 153* (6), 064106.
[21] Baer R, Livshits E, Salzner U (2010) Annu. Rev. Phys. Chem. 61:85-109.
[22] Manna A K, Lee M H, McMahon K L, Dunietz B D (2015) *J Chem. Theory Comput*. *11*, 1110–1117.
[23] Mardirossian N, Head-Gordon M, (2017) *Mol. Phys. 115* (19), 2315–2372.
[24] Slater J C (1974) *The Self-Consistent Field for Molecular and Solids*, *Quantum Theory of Molecular and Solids, Vol. 4*, McGraw-Hill, New York.
[25] Ceperley D M, Alder B J (1980) *Phys. Rev.* 45, 566.
[26] Perdew J P, Burke K, Ernzerhof M (1997) *Phys. Rev. Lett*. 77, 3865.
[27] Becke A D (1988) *Phys. Rev*. A 38, 3098.
[28] Lee C, Yang W, Parr R G (1988) *Phys. Rev*. B 37, 785.
[29] Adamo C, Barone V, J. (1999) *Chem. Phys*. 110, 6158.
[30] Stephens PJ, Devlin FJ, Chabalowski CF, Frisch MJ (1994) *J. Phys. Chem*. 98:11623-11627.
[31] Yanai T, Tew DP, Handy NCA (2004) *Chem. Phys. Lett.* 393: 51-57.
[32] Iikura H, Tsuneda T, Yanai T, Hirao K (2001) *J. Chem. Phys.* 115:3540-3544.
[33] Peach M J G, Benfield P, Helgaker T, Tozer D (2008) *J. Chem. Phys. 128*, 044118.
[34] Campetella M, Maschietto F, Frisch M J, Scalmani G, Ciofini I, Adamo C (2017) *J. Comput. Chem.* 38(25):2151-2156.
[35] Maschietto F, Campetella M, Garcia J S, Adamo C, Ciofini I (2021) *J. Chem. Phys.* 154, 204102.
[36] Le Bahers T, Adamo C, Ciofini I (2011) *J. Chem. Theory Comput*. *7*:2498–2506.
[37] Campetella M, Perfetto A, Ciofini I (2019) *Chem. Phys. Lett*. 714, 81-86.
[38] Huet L, Perfetto A, Muniz-Miranda F, Campetella M, Adamo C, Ciofini I (2020) *J. Chem.Theory Comput*. 16, 7, 4543-4553.
[39] Maschietto F, Garcia J S, Campetella M, Ciofini I (2018) *J. Comput. Chem.* 40, 650-656.
[40] Adamo C, Le Bahers T, Savarese M, Wilbraham L, Garcıa G, Fukuda R, Ehara M, Rega N, Ciofini I (2015) *Coord. Chem. Rev. 304*, 166.
[41] Guido C A., Cortona P, Mennucci B, Adamo C (2013) *J. Chem. Theory Comput. 9*, 3118.
[42] Plasser F, Wormit M, Dreuw A (2014). *J. Chem. Phys*. *141*, 024106
[43] Etienne T, Assfeld X, Monari A (2014) *J. Chem. Theory Comput. 10, 3896-3905*
[44] Plasser F (2020) *J. Chem. Phys*. **152**, 084108.
[45] Koster A M, Geudtner G, Alvarez-Ibarra A, Calaminici P, Casida M E, Carmona-Espindola J, Dominguez V D, Flores-Moreno R, Gamboa G U, Goursot A, Heine T, Ipatov A, De La Lande A, Janetzko F, Del Campo J M, MejiaRodriguez D, Reveles J U, Vasquez-Perez J, Vela A, Zuniga-Gutierrez B, Salahub D R, deMon2k, Version 4 (2016) The deMon developers, Cinvestav, Mexico City.
[46] Koster A M, Geudtner G, Alvarez-Ibarra A, Calaminici P, Casida M E, Carmona-Espindola J, Dominguez V D, Flores-Moreno R, Gamboa G U, Goursot A, Heine T, Ipatov A, De La Lande A, Janetzko F, Del Campo J M, Mejia-Rodriguez D, Reveles J U, Vasquez-Perez J, Vela A, Zuniga-Gutierrez B, Salahub D R, deMon2k, Version 6 (2018) The deMon developers, Cinvestav, Mexico City.
[47] Carmona-Espindola J, Koster A M (2013) *Can. J. Chem* 91(9): 795-803.
[48] Calaminici P et al. (2017) *Handbook of Computational Chemistry* pp 1-67.
[49] Mintmire J W, Dunlap B I (1982) *Phys. Rev*. 25 (1), 88.

[50] Tandiana R, Clavaguera C, Hasnaoui K, Pedroza-Montero J N, de la Lande A (2021) *Theor. Chem. Acc*. 140, 126.
[51] Calaminici P, Janetzko F, Köster A M, Mejia-Olvera R, Zúñiga-Gutiérrez B (2017) J. Chem. Phys. 126, 044108.
[52] de la Lande A, Clavaguera C, Köster A (2017) *J. Mol. Model*. 23, 99.
[53] Fuks J I, Helbig N, Tokatly I V, Rubio A (2011) *Phys. Rev.* B 84, 075107.
[54] Raghunathan S, Nest M (2012) *J. Chem. Theory Comput.* 8,3,806-809.
[55] Rohringer N, Peter S, Burgdorfer J (2006) *Phys. Rev.* A 74, 042512.
[56] Bedurke F, Klamroth T, Saalfrank P (2021) *Phys. Chem. Chem. Phys*. 23, 13544-13560.
[57] Saalfrank P, Bedurke F, Heide C, Klamroth T, Klinkusch S, Krause P, Nest M, Tremblay J C (2020) *Advances in Quantum Chemistry* pp 16-46.
[58] Fowe Penka E, Couture-Bienvenue E, Bandrauk A D (2014) *Phys. Rev.* A 89, 023414.
[59] Alvarez-Ibarra A, Omar KA, Hasnaoui K, de la Lande A (2022) Multiscale Dynamics Simulations: Nano and Nano-bio Systems in Complex Environments *The Royal Society of Chemistry* 117-143.
[60] Magnus W (1954) *Commun. Pure. App. Math*. 7 (4), 649.
[61] Gómez Pueyo A, Marques M A L, Rubio A, Castro A (2018) *J. Chem. Theor. Comput*. 14 (6), 3040.
[62] Cheng, C-L, Evans J S, Van Voorhis T, (2006) *Phys. Rev.* B 74 (15), 155112.
[63] Mulliken R S (1952) *J. Am. Chem. Soc.* 74, 811.
[64] Maschietto F, Campetella M, Frisch M J, Scalmani G, Adamo C, Ciofini I (2018) *J. Comput. Chem*. 39, 735– 742.
[65] Ciofini I, Le Bahers T, Adamo C, Odobel F, Jacquemin D (2012) *J. Phys. Chem*. 116 (22), 11946-11955.